# Production of $\pi^+$ and $K^+$ mesons in 3.2 AGeV argon-nucleus interactions at the Nuclotron

BM@N Collaboration

**Abstract**

First physics results of the BM@N experiment at the Nuclotron/NICA complex are presented on $\pi^+$ and $K^+$ meson production in interactions of the 3.2 AGeV argon beam with fixed targets. Transverse momentum, rapidity spectra and multiplicities of $\pi^+$ and $K^+$ mesons are measured. The results are compared with predictions of theoretical models and with the measurements from heavy ion experiments at lower energies.

# 1 Introduction

BM@N (baryonic matter at Nuclotron) is the first experiment operational at the ion-accelerating complex Nuclotron/NICA, studying interactions of relativistic beams of heavy ions with fixed targets [1] in the energy range of high densities of baryonic matter [2]. At the Nuclotron energies, the density of nucleons in a fireball created by two colliding heavy nuclei is 3-4 times higher than the nuclear saturation density [3]. In addition, these energies are high enough to study strange mesons and (multi)-strange hyperons produced in nucleus-nucleus collisions close to the kinematic threshold [4, 5]. The primary goal of the experiment is to constrain parameters of the equation of state (EoS) of high-density nuclear matter. Studies of the excitation function of strange particle production below and near to the kinematical threshold make it possible to distinguish hard behaviour of the EoS from the soft one [6].

The Nuclotron will provide the experiment with beams of a variety of particles, from protons to gold ions, with kinetic energy in the range from 1 to 6 GeV/nucleon for light ions with Z/A ratio of $\sim 0.5$ and up to 4.5 GeV/nucleon for heavy ions with Z/A ratio of $\sim 0.4$.

Recently BM@N collected first experimental data in beams of carbon, argon, and krypton ions [7, 8]. This paper presents first results on $\pi^+$ and $K^+$ meson production in 3.2 AGeV argon-nucleus interactions. The experimental data correspond to an integrated luminosity of 7.8 $\mu\mathrm{b}^{-1}$ collected with different targets: 2.1 $\mu\mathrm{b}^{-1}$ (C), 2.3 $\mu\mathrm{b}^{-1}$ (Al), 1.8 $\mu\mathrm{b}^{-1}$ (Cu), 1.1 $\mu\mathrm{b}^{-1}$ (Sn), 0.5 $\mu\mathrm{b}^{-1}$ (Pb).

The paper is organized as follows. Section 2 describes the experimental set-up and section 3 is devoted to details of the event reconstruction. Section 4 describes the evaluation of the $\pi^+$, $K^+$ reconstruction efficiency. Experimental results on transverse momentum, rapidity spectra and multiplicities of $\pi^+$ and $K^+$ mesons are given in section 5. The BM@N measurements are compared with predictions of theoretical models and with experimental data on medium-sized nucleus-nucleus interactions measured at lower energies. Finally, the results are summarized in section 6.

# 2 Experimental set-up

The BM@N detector is a forward spectrometer covering the pseudorapidity range $1.6 \leq \eta \leq 4.4$. Schematic view of the BM@N setup in the argon-beam run is shown in figure 1. More details of all components of the set-up are described

in [9]. The spectrometer includes a central tracking system consisting of 3 planes of forward silicon- strip detectors (ST) and 6 planes of detectors based on gas electron multipliers (GEM) [10]. The central tracking system is located downstream of the target region inside of a dipole magnet with the bending power of about $\approx 2.1$Tm.

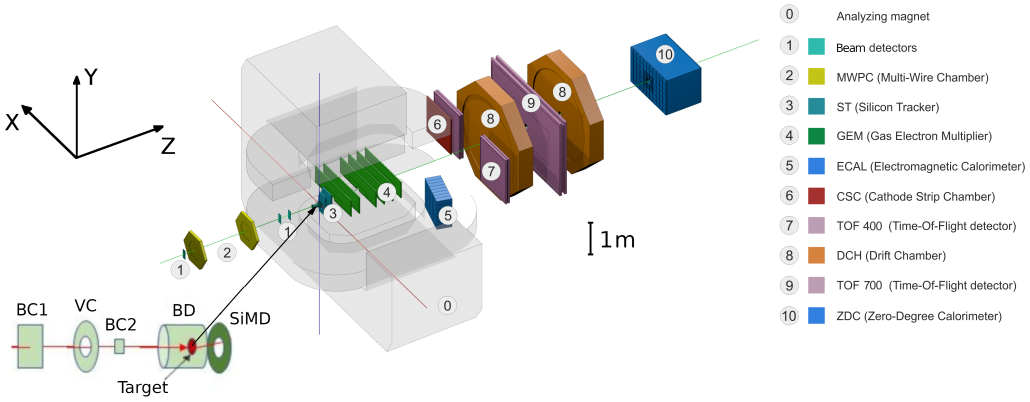


Figure 1: Schematic view of the BM@N setup in the argon-beam run.

Outer drift chambers (DCH), a cathode strip chamber (CSC), two sets of time-of-flight detectors (ToF) and a zero degree calorimeter (ZDC) are located downstream the dipole magnet. The tracking system measures of momenta p of charged particles with a relative uncertainty that varies from 2.5% at the momentum of 0.5 GeV/c to 4.5% at 3.5 GeV/c as it is shown in figure 2.

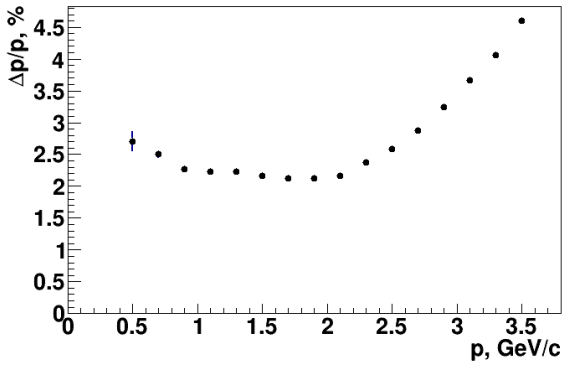


Figure 2: Relative momentum resolution as a function of the momentum.

The primary collision vertex position (PV) is measured with a resolution of 2.4 mm in the X-Y plane perpendicular to the beam direction and 3 mm in the beam direction at the target position. The distribution of the primary vertices along the beam direction ($Z_{ver}$) for experimental data and Monte Carlo events is shown in figure 7e. Different types of charged hadrons are identified by two ToF systems.

The event triggering is performed by a combination of signals of two beam counters (BC1, BC2), a veto counter (VC), a barrel detector (BD) and a silicon multiplicity detector (SiMD). The BC2 counter was used as a start trigger T0. The BD detector consists of 40 azimuthal scintillating strips arranged around the target, and the SiMD detector consists of 60 azimuthal silicon segments situated behind the target.

To count the number of beam ions that passed through the target, a logical beam trigger BT = BC1$\otimes\overline{\text{VC}}\otimes$BC2 was used. The following logic conditions were applied to generate the trigger signal: 1) BT$\otimes$(BD$\geq 3, 4$); 2) BT$\otimes$(SiMD$\geq 3, 4$); 3) BT$\otimes$(BD$\geq 2$)$\otimes$(SiMD$\geq 3$). The trigger conditions were varied to find the optimal ratio between the event rate and the trigger efficiency for each target. Trigger condition 1 was applied for 60% of data collected with the carbon target. This trigger fraction was continuously reduced with the atomic weight of the target down to 26% for the Pb target. The fraction of data collected with trigger condition 2 was rising from 6% for the carbon target up to 34% for the Pb target. The rest of data were collected with trigger condition 3.

The data from the forward silicon detectors, GEM detectors, outer drift chambers, cathode strip chamber and two sets of the time-of-flight detectors ToF-400 [33] and ToF-700 [34] were used for the analysis. The time resolutions of the ToF-400 and ToF-700 systems are 84 ps and 115 ps, respectively [35]. For argon-nucleus collisions at 3.2 AGeV, 83M events were analysed.

The research program of the run was devoted to measurements of inelastic reactions $Ar + A \rightarrow X$ with the argon beam intensity of a few $10^5$ ions per spill and a spill duration of 2–2.5 sec. A set of solid targets of various materials (C, Al, Cu, Sn, Pb) with a relative interaction length of 3% was used.

# 3 Event reconstruction

Track reconstruction in the central tracker is based on a "cellular automaton" approach [11] implementing a constrained combinatorial search of track candidates with their subsequent fitting by a Kalman filter to determine track parameters. These tracks are used to reconstruct primary (interaction) and secondary (decay)

vertices and global tracks by extrapolation to the downstream detectors (CSC, DCH and ToF) and matching with their measurements.

Charged mesons ($\pi^+$ and $K^+$) were identified using the time of flight $\Delta t$ measured in T0 and ToF detectors, the length of the trajectory $\Delta l$ and the momentum $p$ reconstructed in the central tracker. Than the squared mass $M^2$ of a particle is calculaed by the formula: $M^2 = p^2((\Delta tc/\Delta l)^2 - 1)$, where $c$ is the speed of light. Candidates of $\pi^+$ and $K^+$ must originate from the primary vertex and match hits in CSC and ToF-400 or in the DCH and ToF-700 detectors.
The criteria for selecting of $\pi^+$ and $K^+$ meson candidates were the following:

- Each track has at least 4 hits in the GEM detectors (6 detectors in total) [10]. Hits in the forward silicon detectors were used to reconstruct the track, but no requirements were applied to the number of hits;

- Tracks originate from the primary vertex. The deviation of the reconstructed vertex from the target position along the beam direction is limited to -3.4 cm $< Z_{\rm ver} - Z_0 <$ 1.7 cm, where $Z_0$ is the target position. The upper limit corresponds to $\sim 5.7\sigma$ of the $Z_{ver}$ spread and cuts off interactions with the trigger detector located 3 cm behind the target (see figure 7e). Two vertical lines in figure 7e) limit the region of the Z coordinate accepted for the data analysis for all the targets.

- Distance from a track to the primary vertex in the X-Y plane at $Z_{\rm ver}$ (DCA) is required to be less than 1 cm, which corresponds to 4 $\sigma$ of the vertex resolution in the X-Y plane;

- Momentum range of positively charged particles $p > 0.5$ GeV/c and $p > 0.7$ GeV/c is limited by the acceptance of the ToF-400 and ToF-700 detectors, respectively;

- Distance of extrapolated tracks to the CSC (DCH) hits as well as to the ToF-400 (ToF-700) hits should be within $\pm 2.5\sigma$ of the hit-track residual distributions and depends upon the track momentum range as shown in figure 3.

The spectra of the mass squared ($M^2$) of positively charged particles produced in interactions of the 3.2 AGeV argon beam with various targets are shown in figures 4a and 4b for ToF-400 and ToF-700 data, respectively. The $\pi^+$ and $K^+$ signals were extracted in the $M^2$ windows from -0.09 to 0.13 (GeV/c$^2$)$^2$ and from 0.18 to 0.32 (GeV/c$^2$)$^2$, respectively. The signals of $\pi^+$ and $K^+$ and

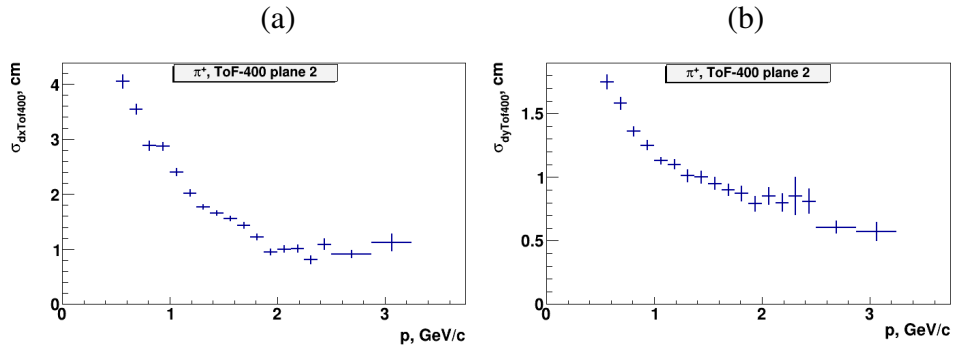


Figure 3: Width of the Gaussian fit of the ToF-400 hit residuals with respect to positively charged tracks depending on the particle momentum: projection X (a), Y (b).

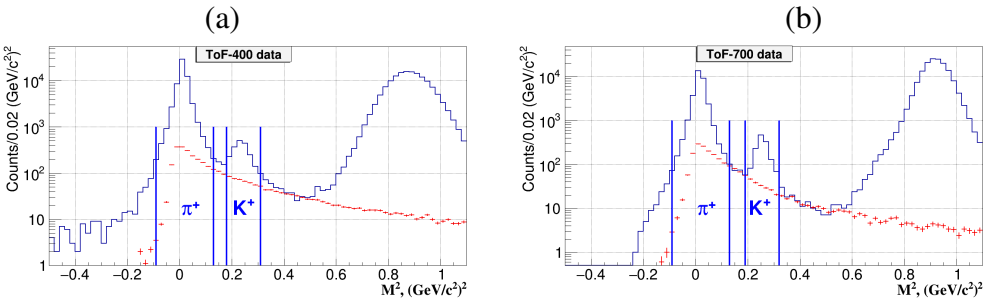


Figure 4: $M^2$ spectra of positively charged particles produced in argon-nucleus interactions and measured in the ToF-400 (a) and ToF-700 (b) detectors. Vertical lines show the signal ranges of selected $\pi^+$ and $K^+$ mesons. Red points with error bars show the the background estimated from "mixed events".

statistical errors were calculated according to the formulae: $sig = hist - bg$, $err_{stat} = \sqrt{hist + bg}$, assuming the background uncertainty of $\sqrt{bg}$. Here $hist$ and $bg$ denote the histogram integral and the background integral within the $M^2$ windows of $\pi^+$ and $K^+$ mesons.

The shape of the background under the $\pi^+$ and $K^+$ signals in the $M^2$ spectra was estimated using the "mixed event" method. For that, tracks reconstructed in the central tracker were matched to hits in the ToF detectors taken from independent events. The "mixed event" background was normalized to the integral of the signal histogram outside the $M^2$ windows of $\pi^+$ and $K^+$ mesons, i.e in the $M^2$ ranges 0.13-0.18 $(\text{GeV/c}^2)^2$ and 0.32-0.4 $(\text{GeV/c}^2)^2$. It was found that the background level differs when the beam interacts with light and heavy targets and for different intervals of the rapidity and transverse momentum.

To estimate the systematic errors of the $\pi^+$ and $K^+$ signals due to the background subtraction method, the $M^2$ distributions were parameterised using a linear fit in the $M^2$ range -0.14-0.4 (GeV/c$^2$)$^2$. The $M^2$ windows of the $\pi^+$ and $K^+$ signals were excluded from the linear fit. The difference between the background integral under the $\pi^+$ and $K^+$ signals taken from "mixed events" and the $bg$ integral taken from the fitting of the $M^2$ spectra was used as a systematic error.

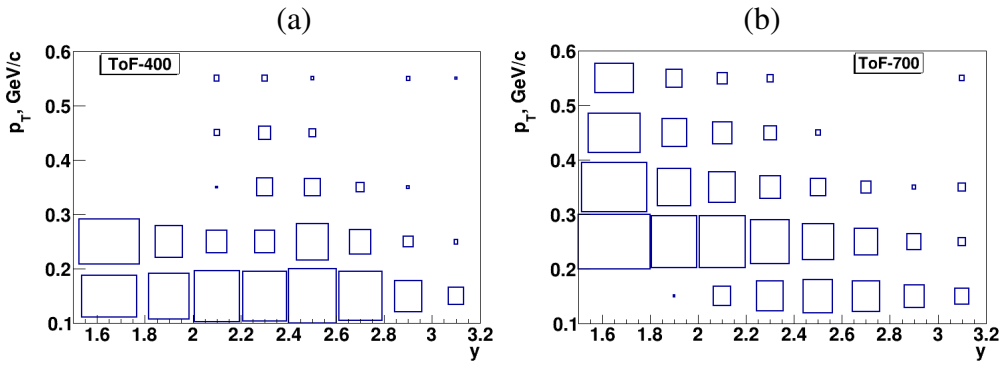


Figure 5: Distribution of the $\pi^+$ signals measured in ToF-400 (a) and ToF-700 (b) in the rapidity and transverse momentum bins in Ar+Sn interactions.

The acceptances of the ToF-400 and ToF-700 detectors cover different ranges of the rapidity and transverse momentum of detected particles. Figure 5 shows coverage of the phase space of the $\pi^+$ signals measured in ToF-400 and ToF-700 in the rapidity and transverse momentum intervals in Ar+Sn interactions before making corrections for the efficiency.

# 4 Efficiency of event reconstruction and trigger performance

Monte Carlo data samples of argon-nucleus collisions were produced with the DCM-SMM event generator [12, 13]. Propagation of particles through the entire detector volume and responses of the detectors were simulated using the GEANT3 program [14] integrated into the BmnRoot software framework [15]. To properly describe the GEM detector response in the magnetic field, the Garfield++ toolkit [16] for simulation of the micropattern gaseous detectors was used.

The efficiencies of the forward silicon, GEM, CSC, DCH and ToF detectors were adjusted during simulation in accordance with the detector efficiencies mea-

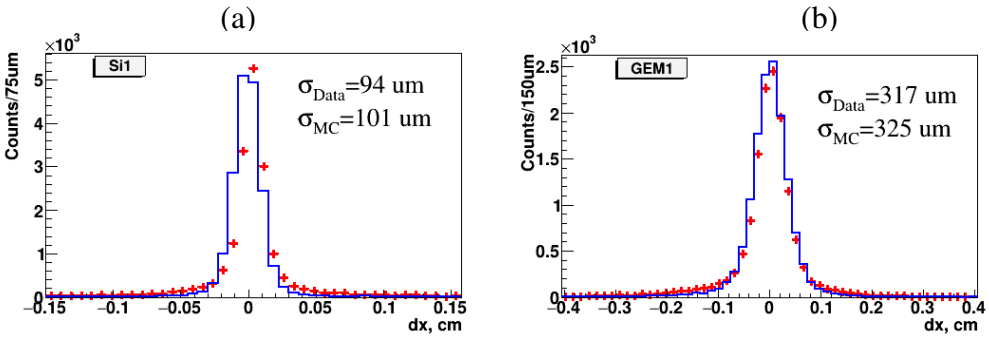


Figure 6: Residual distributions of hits in the X projection (magnet deflection plane) with respect to reconstructed tracks: (a) - in the first forward silicon plane, (b) - in the first GEM plane. The experimental data are shown as red crosses, and the simulated data are shown as blue histograms.

sured in the experimental events. The Monte Carlo events went through the same chain of reconstruction and identification as the experimental events.

The level of agreement between the Monte Carlo and experimental distributions is demonstrated on a set of observables: hit-track residuals in the central tracker detectors, distance from a track to the primary vertex in the X-Y plane at $Z_{ver}$ (DCA), $\chi^2$/NDF, number of tracks reconstructed at the primary vertex and number of hits per track (see figures 6 and 7a–d).

The $\pi^+$ and $K^+$ reconstruction efficiency is estimated in the intervals of rapidity $y$ and transverse momentum $p_T$. It takes into account the geometrical acceptance, the detector efficiency, the kinematic and spatial cuts efficiency and loss of $\pi^+$ and $K^+$ due to decays on the fly. The reconstruction efficiencies of $\pi^+$ detected in ToF-400 and ToF-700 are shown in figure 8 in the $y$ and $p_T$ intervals for Ar+Sn interactions.

The efficiency to get a trigger signal based on multiplicities of fired channels in the BD (SiMD) detectors $\epsilon_{trig}$ was calculated for events with reconstructed $\pi^+$ and $K^+$ mesons using experimental event samples recorded with an independent trigger based on the SiMD (BD) detectors. The BD and SiMD detectors cover different parts of the acceptance of the BM@N setup, that is, they detect different products of an interaction. For the BD trigger efficiency estimation, the following relation was used: $\epsilon_{trig}$ (BD $\geq$ m) = N(BD $\geq$ m $\otimes$ SiMD $\geq$ n)/N(SiMD $\geq$ n), where m and n are the minimum number of fired channels in BD (m = 3, 4) and SiMD (n = 3, 4) (see section 2). A similar relation was applied to evaluate the SiMD trigger efficiency. The BD (SiMD) trigger efficiency is averaged over all

data with the minimum number of fired channels in SiMD (BD). To estimate a possible distortion of $\epsilon_{trig}$ (BD $\geq$ m) due to selection of events with the hardware-set condition N(SiMD $\geq$ n), $\epsilon_{trig}$ was also evaluated in the limited amount of events registered with the beam trigger BT. The difference between the results was treated as one source of the systematic uncertainty of the trigger efficiency. The efficiency for combined BD and SiMD triggers was calculated as the product of the efficiencies of BD and SiMD triggers. The systematic uncertainty of this factorization assumption was estimated from the difference of $\epsilon_{trig}$ with the result evaluated in events registered with the beam trigger BT. The dependences of the trigger efficiency on the track multiplicity in the primary vertex and the X/Y vertex position were also taken into account. The systematic uncertainties estimated in the analysis cover variations in the trigger efficiency as a function of the number of on-vertex tracks and position of the primary vertex relative to the mean value of trigger efficiency. The total systematic uncertainty of the trigger efficiency was calculated as the quadratic sum of uncertainties from different sources. The trigger efficiency averaged over all data collected with the trigger conditions 1) BD$\geq 3, 4$; 2) SiMD$\geq 3, 4$; 3) (BD$\geq 2$)$\otimes$(SiMD$\geq 3$) (see section 2) is shown in Fig.9 as a function of the event centrality estimated from the simulation. The measurements cover the entire range of event centralities, but the trigger efficiency was lower for peripheral interactions than for central and semi-central collisions.

# 5 Calculation of yields and uncertainties

The differential cross sections $d^2\sigma_{\pi,K}(y,p_T)/dydp_T$ and yields $d^2N_{\pi,K}(y,p_T)/dydp_T$ of $\pi^+$ and $K^+$ meson production in Ar+C, Al, Cu, Sn, Pb interactions are calculated in bins of $(y,p_T)$ by the formulas:

$$d^2\sigma_{\pi,K}(y,p_T)/dydp_T = d^2n_{\pi,K}(y,p_T)/(\epsilon_{rec}(y,p_T)\epsilon_{trig}Ldydp_T)$$
$$d^2N_{\pi,K}(y,p_T)/dydp_T = d^2\sigma_{\pi,K}(y,p_T)/(\sigma_{inel}dydp_T) \quad (1)$$

where $L$ is the luminosity, $n_{\pi,K}$ is the number of reconstructed $\pi^+$ and $K^+$ mesons in intervals $dy$ and $dp_T$, $\epsilon_{rec}$ is the efficiency of the $\pi^+$ and $K^+$ meson reconstruction, $\epsilon_{trig}$ is the trigger efficiency, $\sigma_{inel}$ is the cross section for inelastic argon-nucleus interactions. The cross sections for inelastic Ar+C, Al, Cu, Sn, Pb interactions are taken from the predictions of the DCM-SMM model which are consistent with the results calculated by the formula: $\sigma_{inel} = \pi R_0^2(A_P^{1/3} + A_T^{1/3})^2$, where $R_0 = 1.2$ fm is the effective nucleon radius, $A_P$ and $A_T$ are the atomic numbers of the projectile and target nucleus [29]. The uncertainties for the Ar+C, Al, Cu, Sn, Pb inelastic cross sections are estimated from an alternative for-

mula ( [20]) which approximates the measured nucleus-nucleus cross sections: $\sigma_{inel} = \pi R_0^2 (A_P^{1/3} + A_T^{1/3} - b)^2$ with $R_0 = 1.46$ fm and $b = 1.21$ The values and uncertainties of $\sigma_{inel}$ for Ar+C, Al, Cu, Sn, Pb interactions used to estimate the yields of $\pi^+$ and $K^+$ mesons are given in table 2.

The yields of $\pi^+$ ($K^+$) mesons in Ar+C, Al, Cu, Sn, Pb interactions are measured in the kinematic range of the transverse momentum of $\pi^+$ ($K^+$) meson $0.1 < p_T < 0.6$ GeV/c ($0.1 < p_T < 0.5$ GeV/c) and the $\pi^+$ ($K^+$) meson rapidity in the laboratory frame $1.5 < y < 3.2$ ($1.0 < y < 2.0$). The systematic error of the $\pi^+$ and $K^+$ meson yield in each $p_T$ and $y$ bin is calculated as the quadratic sum of the uncertainties from the following sources:

- Sys1: systematic errors of the reconstruction efficiency due to the remaining difference in the X/Y distribution of primary vertices in the simulation relative to experimental data.

- Sys2: systematic errors of the background subtraction under the $\pi^+$ and $K^+$ signals in the mass-squared spectra of identified particles as described in section 3. This uncertainty affects the number of reconstructed $\pi^+$ and $K^+$ in $p_T$ and $y$ bins in data as well as in simulated events. As a result its effect is smaller for the $\pi^+$ and $K^+$ yields calculated by formula (1).

- Sys3: systematic error of the trigger efficiency estimated as a function of the number of tracks from the primary vertex and the X/Y position of primary vertex.

In addition to uncertainties Sys1-Sys3, uncertainties of the normalization of the $\pi^+$ and $K^+$ yields were estimated. The normalization uncertainty is calculated as the quadratic sum of the uncertainty of the trigger efficiency, uncertainties of the tracking detector efficiency, efficiency of the track matching to the CSC (DCH) outer detectors and to ToF-400 (ToF-700), uncertainties of the luminosity and inelastic nucleus-nucleus cross section. These uncertainties are calculated for the entire measured $(y, p_T)$ range, i.e. they are treated as fully correlated in all bins of $y$ and $p_T$. The luminosity uncertainty is estimated to be within 2%. It corresponds to the fraction of the beam which can miss the target, estimated from the vertex positions of the data. The uncertainty of the trigger efficiency is 28% for detecting $K^+$ in Ar+C interactions and between 7.5% (Ar+Al) and 4% (Ar+Pb) for detecting $K^+$ in interactions of argon ions with heavier targets. The uncertainty of the trigger efficiency for the $\pi^+$ detection ranges between 4.5% (Ar+C) and 0.9% (Ar+Pb). The uncertainty of the central tracking detector efficiency is

estimated to be within 3%. Its effect is estimated from the remaining difference in the number of track hits in the central detectors in the simulation relative to the experimental data (see figure 7d). Combined systematic uncertainty of matching of extrapolated tracks to the CSC (DCH) hits and ToF-400 (ToF-700) hits is within 5%. It is estimated from the remaining difference in the matching efficiency in the simulation relative to the experimental data. Table 1 summarizes the total systematic uncertainty from the sources Sis1 - Sis3 and the uncertainty of normalization of the $\pi^+$ and $K^+$ yields.

Table 1: Systematic uncertainties of the $\pi^+$ and $K^+$ yields measured in argon-nucleus interactions.

| Reaction / Systematics | Ar+C sys% | Ar+Al sys% | Ar+Cu sys% | Ar+Sn sys% | Ar+Pb sys% |
|---|---|---|---|---|---|
| Sys1, $\pi^+$ | 7 | 6 | 6 | 4 | 4 |
| Sys2, $\pi^+$ | 11 | 8 | 9 | 7 | 7 |
| Sys3, $\pi^+$ | 7 | 7 | 7 | 7 | 7 |
| Norm (trigger + tracking + luminosity), $\pi^+$ | 7.8 | 6.3 | 6.2 | 6.2 | 6.2 |
| Sys1, $K^+$ | 15 | 14 | 7 | 7 | 9 |
| Sys2, $K^+$ | 19 | 18 | 11 | 9 | 11 |
| Sys3, $K^+$ | 14 | 12 | 7 | 7 | 7 |
| Norm (trigger + tracking + luminosity), $K^+$ | 29 | 10 | 8.4 | 7.6 | 7.4 |

# 6 Results and discussion

The differential $y$ spectra of the $\pi^+$ and $K^+$ meson yields are calculated in the $p_T$ bins using formulae (1) and are shown in figures 10 and 11, respectively. The measurements correspond to the forward and central rapidity range in the nucleon-nucleon centre of mass CM system because the rapidity of the nucleon-nucleon CM system is $y_{CM} = 1.08$ for the 3.2 GeV/nucleon beam kinetic energy. Predictions of the DCM-SMM [12, 13], UrQMD [18] and PHSD [19] models are shown for comparison. Although the DCM-SMM model was used to estimate the reconstruction efficiency (section 4), model's predictions as such, may well differ from the measurement results. All three models predict a flatter behaviour of the $\pi^+$ spectra as a function of rapidity at low $p_T$ compared to with the experiment.

The experimental spectra of $\pi^+$ are 1.5 times lower than the model predictions for the production of $\pi^+$ in Ar+C interactions. All three models predict higher multiplicities of $K^+$ at low $p_T$ than those measured in the experiment. But the difference is smaller at larger values of $p_T$. The DCM-SMM model predicts a higher $K^+$ multiplicity at low $p_T$ and rapidity compared to PHSD, whereas the UrQMD predictions are lower than PHSD at low $p_T$. The $p_T$ spectra of $\pi^+$ and $K^+$ mesons are measured in the bins of rapidity $y$ and are shown in figures 12 and 13, respectively. Due to low statistics of the $K^+$ meson signal in Ar+C interactions, the results are given only for the entire measured range in $y$ and $p_T$. The $p_T$ spectra of $K^+$ mesons over the entire measured rapidity range are shown in figure 14. In figures 12, 13 and 14 the measured $p_T$ spectra of $\pi^+$ and $K^+$ mesons are parameterised by the form:

$$1/p_T \cdot d^2N/dydp_T \propto \exp(-(m_T - m_{\pi,K})/T_0),$$

where $m_T = \sqrt{m^2_{\pi,K} + p^2_T}$ is the transverse mass, $dy$ is the width of $y$ bin, $dp_T$ is the width of $p_T$ bin, the inverse slope parameter $T_0$ – free fitting parameter. The values of the inverse slope $T_0$, determined from the fits of the $p_T$ spectra of $\pi^+$ and $K^+$ mesons are given in figures 15 and 16, respectively. The value of $T_0$ measured for $\pi^+$ mesons produced in argon-nucleus interactions at the 3.2 AGeV beam kinetic energy is about 40 MeV in the forward rapidity range, rising to 90 MeV in the central rapidity range. In general, the $y$ dependence of the fitting results for $\pi^+$ mesons is consistent with the predictions of the DCM-SMM, UrQMD and PHSD models, but the results of BM@N measurements give a flatter dependence of the $T_0$ values in the central rapidity range compared to the rising dependence of the inverse slopes predicted by the models. The $T_0$ values measured in 3 $y$ bins for $K^+$ mesons have large statistical and systematic errors (see figure 16), but the slope dependence on $y$ is rather weak. The $T_0$ values obtained for the entire measured range of $1.0 < y < 2.0$ are consistent within the errors with 80 MeV for all the targets (see table 3). The weak dependence of the slope $T_0$ is reproduced by all three models, but UrQMD predicts 2 times larger values compared to the measurement. Measured values of $\pi^+$ and $K^+$ meson multiplicities in the interactions of Ar+C, Al, Cu, Sn, Pb are extrapolated to the entire kinematic range using the averaged values of the extrapolation coefficients from the predictions of the DCM-SMM, UrQMD and PHSD models which are shown in table 2. The maximal differences of the predictions of the models from the averaged values are taken as the uncertainties of the extrapolation coefficients. The multiplicities of $K^+$ and $\pi^+$ mesons and their ratios are summarized in table 3. The ratios of the $K^+$ to $\pi^+$ multiplicities do not show a significant dependence on the mean number

of participant nucleons, $A_{\rm part}$, in argon-nucleus collisions shown in table 2. The values of $A_{\rm part}$ are calculated based on the predictions of the DCM-SMM model.

The results of BM@N on the $\pi^+$ and $K^+$ multiplicities are compared with predictions of the DCM-SMM, UrQMD and PHSD models in figures 17a,b. The measured ratios of the $\pi^+$ and $K^+$ meson multiplicities to $A_{\rm part}$ decrease with the increasing atomic weight of the target from Al to Pb. The result for $\pi^+$ in Ar+C interactions is below the results for heavier targets. The ratios of the $K^+$ to $\pi^+$ multiplicities are given in figure 17c. They show no dependence on the number of participant nucleons. The PHSD prediction is compatible with this result, whereas the DCM-SMM and UrQMD models predict smooth rising of the $K^+$ to $\pi^+$ ratio with $A_{\rm part}$.

The $\pi^+$ and $K^+$ meson multiplicities in argon-nucleus interactions can be compared with the previous results of the HADES experiment measured Ar+KCl interactions at the lower beam kinetic energy of 1.76 AGeV [21–23] and with the FOPI experiment, in which Ni+Ni interactions were measured at the beam kinetic energy of 1.93 AGeV [24–26]. The KaoS experiment also measured the $K^+$ multiplicities in Ni+Ni interactions at the beam kinetic energies of 1.5 and 1.93 AGeV [27, 28] which are consistent with the results of the FOPI experiment. The HADES experiment measured the total multiplicities of $\pi^-$ and $K^+$ in semi-central events (the mean number of participant nucleons $A_{\rm part}$ is 38.5) of 3.9 and $2.8 \cdot 10^{-2}$, respectively. The effective inverse slope parameters of the $m_T$ spectra of $\pi^-$ and $K^+$ extrapolated to $y^* = 0$ are 82.4 MeV and 89 MeV, respectively. The BM@N results on the $K^+$ and $\pi^+$ multiplicities at the beam kinetic energy of 3.2 AGeV in Ar+Cu interactions ($A_{\rm part}$ of 33.6, see table 2) are higher by factors of 5 and 1.3 relative to the results for kaons and pions measured by HADES. The difference in the $K^+$ multiplicities could be explained by the energy dependence of the $K^+$ cross section near the kinematical threshold for $K^+$ production ($E_{thr}(NN) \sim 1.58$ GeV). The inverse slope parameters $T_0$ measured for $\pi^+$ and $K^+$ in the central rapidity range (see figures 15 and 16) are comparable to the HADES results.

The FOPI experiment measured the total multiplicities of $K^+$ in triggered semi-central Ni+Ni interactions ($A_{\rm part}$ of 46.5) and central events ($A_{\rm part}$ of 75) of $3.6 \cdot 10^{-2}$ and $8.25 \cdot 10^{-2}$, respectively. These values can be compared with the BM@N results presented in table 3 for various targets. The $K^+/\pi^+$ multiplicity ratio measured by FOPI in triggered semi-central events is $7.6 \cdot 10^{-3}$, which is by a factor 3 smaller than the $K^+/\pi^+$ multiplicity ratio obtained by BM@N in Ar + Sn interactions for the entire kinematical range ($A_{\rm part}$ of 48.3, see table 2). It should be taken into account that the beam kinetic energy of the FOPI experiment

(1.93 AGeV) is lower than that of the BM@N experiment. The effective inverse slope of 110.9 MeV, estimated by FOPI at $y^* = 0$ from the $K^+$ transverse mass spectrum is consistent within the uncertainties with the inverse slope parameter $T_0$, measured by BM@N for $K^+$ in the range $y^* \gtrsim 0$. The consistency of the transverse momentum slopes measured by BM@N with the results of the HADES and and FOPI experiments indicates the absence of a strong dependence on the beam energy and atomic weights of colliding nuclei.

Multiplicities of pions in the entire kinematic range $N_\pi^{tot}$, where $N_\pi^{tot} = N_{\pi^+}^{tot} + N_{\pi^-}^{tot} + N_{\pi^0}^{tot}$, normalized to the average number of participant nucleons $A_{\rm part}$ are compiled in figure 18 for different colliding nuclei and beam energies. References [36] and [37] contain compilation of the pion data for interactions of nucleon-nucleon (N+N) [38], Mg+Mg [39], La+La [40], Au+Au [41–43], Ar+KCl [44], Si+Al, S+S [45, 46], Pb+Pb [47, 55], Au+Au [48–51]. To estimate $N_\pi^{tot}$ from the $\pi^+$ multiplicities measured by BM@N, the predictions of the DCM-SMM model are used. Multiplicities of $K^+$ in the entire kinematic range normalized to the average number of participant nucleons $A_{\rm part}$ are compiled in figure 19. The world data taken from [24, 52–55] are compared with the results of the BM@N experiment. Figures 18 and 19 show that the BM@N results are consistent with the world data on the production of $\pi$ and $K^+$.

# 7 Summary

First physics results of the BM@N experiment are presented for the $\pi^+$ and $K^+$ meson yields and their ratios in argon-nucleus interactions at the beam kinetic energy of 3.2 AGeV. The results obtained are compared with the DCM-SMM, UrQMD and PHSD models of nucleus-nucleus interactions and with the results of other experiments in which nucleus-nucleus interactions at lower energies were studied.

The value of the inverse slope of the transverse momentum spectrum measured for $\pi^+$ mesons is about 40 MeV in the forward rapidity range, rising to 90 MeV in the central rapidity range. In general, the y- dependence of the fitting results for $\pi^+$ mesons is consistent with the predictions of the models, but there is a tendency that BM@N measures a flatter dependence of the slope values in the central rapidity range compared to a rising dependence predicted by the models.

The ratios of the $K^+$ to $\pi^+$ multiplicities show no significant dependence on the mean number of participant nucleons $A_{\rm part}$ of argon-nucleus collisions. The PHSD prediction is compatible with the BM@N result, whereas the DCM-SMM

and UrQMD models predict smooth rising of the $K^+$ to $\pi^+$ ratio with $A_{\rm part}$.

The $\pi^+$ and $K^+$ multiplicities measured by BM@N normalized on $A_{\rm part}$ are found to be consistent with the rising energy dependence of the world data on the production of $\pi^+$ and $K^+$ mesons measured for various colliding nuclei and beam energies.

**Acknowledgments.** The BM@N Collaboration acknowledges support of the HybriLIT of JINR, HPC Village project and HGPU group for the provided computational resources.

# References

[1] M. Kapishin (for the BM@N Collaboration), Eur. Phys. J. A52 (2016) no. 8, 213.

[2] J. Randrup and J. Cleymans, Phys. Rev. C 74 (2006) 047901.

[3] B. Friman, W. N*ö*renberg, and V.D. Toneev, Eur. Phys. J. A 3 (1998).

[4] NICA White Paper, Eur. Phys. J. A 52 (2016).

[5] BM@N Conceptual Design Report:
http://nica.jinr.ru/files/BM@N/BMN_CDR.pdf

[6] Ch. Fuchs, Prog. Part. Nucl. Phys. 56 (2006) 1-103.

[7] M. Kapishin (for the BM@N Collaboration), Nucl. Phys. A 982 (2019) 967-970.

[8] M. Kapishin (for the BM@N Collaboration), SQM 2019 proceedings, 285 Springer Proc. Phys. 250 (2020) 21-27.

[9] BM@N project:
http://nica.jinr.ru/files/BM@N/BMN_project.pdf

[10] D. Baranov et al., JINST 12 (2017) no. 06, C06041 .

[11] V. Akishina and I. Kisel, J. Phys.: Conf. Ser. 599, 012024 (2015), I. Kisel, Nucl. Instrum. Meth. A 566, 85 (2006).

[12] N. Amelin, K. Gudima, and V. Toneev, Sov. J. Nucl. Phys. 51, 1093 (1990).

[13] M. Baznat, A. Botvina, G. Musulmanbekov, V. Toneev, V. Zhezher, Phys. Part. Nucl. Lett. 17 (2020) no. 3; arXiv: 1912.09277v.

[14] CERN Program Library, Long Writeup W5013, Geneva, CERN, 1993.

[15] https://git.jinr.ru/nica/bmnroot

[16] http://garfieldpp.web.cern.ch/garfieldpp

[17] D. Baranov et al., Phys. Part. Nucl. Lett. 15 (2018) no. 2, 148-156.

[18] S. A. Bass et al., Prog. Part. Nucl. Phys. 41 225 (1998).

[19] W. Cassing and E. L. Bratkovskaya, Nucl. Phys. A 831 (2009) 215-242.

[20] H. Angelov et al., P1-80-473, JINR, Dubna.

[21] G. Agakishiev et al., HADES Collaboration, Eur. Phys. J. A 47 (2011) 21.

[22] G. Agakishiev et al., HADES Collaboration, Phys. Rev. C 80 (2009) 025209.

[23] G. Agakishiev et al., HADES Collaboration, Phys. Rev. C 82 (2010) 044907.

[24] D. Best et al., FOPI Collaboration, Nucl. Phys. A 625 (1997) 307-324.

[25] N. Bastid et al., FOPI Collaboration, Phys. Rev. C 76 (2007) 024906.

[26] K. Piasecki et al., FOPI Collaboration, Phys. Rev. C 99 (2019) 1, 014904.

[27] M. Menzel et al., KaoS Collaboration, Phys. Lett. B 495 (2000) 26-32.

[28] A. Forster et al., KaoS Collaboration, Phys. Rev. C 75 (2007) 024906.

[29] K. Kanaki, PhD Thesis, Technische Universit*ä*t Dresden, 2007.

[30] Yu. Kovalev et al., 2017 JINST 12 C07031; B. Topko et al., in IEEE Transactions on Nuclear Science, vol. 69, no. 1, pp. 98-104, Jan. 2022; Topko, B. L. et al., Phys. Part. Nuclei 53, 639–643 (2022); Yu. Topko et al., Nucl. Instrum. Meth. A 1033, 166680 (2022) .

[31] A. Galavanov et al., EPJ Web Conf. 204 (2019) 07009; A. Galavanov et al., 2020 JINST15 C09038.

[32] M. Kapishin et al., EPJ Web Conf., 173 (2018) 04008; E. Mazzucato, Nucl. Phys. B 59 (1997) 174-181.

[33] V. Babkin et al., Nucl. Instrum. Meth. A 824, P.490–492 (2016); V. Babkin et al., Proceedings of Science, 2014, Vol.213 (Proceedings of TIPP-2014), P.289 .

[34] N. Kuzmin et al., Nucl. Instrum. Meth. A 916, P. 190–194 (2019) .

[35] K. Alishina et al., Phys. Part. Nucl., 53 (2022) no. 2, 470-475.

[36] P. Senger et al., J. Phys. G 25 (1999) R59-R131.

[37] J. Adamczewski-Musch et al., Eur. Phys. J. A 56 (2020) 259.

[38] Gazdzicki M. and Röhrich D., 1995 Z. Phys. C 65 215.

[39] Anikina et al., JINR Rapid Comm Dubna, 1 (1989) 12.

[40] Harris J. W. et al., 1987 Phys. Rev. Lett. 58 463.

[41] Pelte D. et al., 1997 Z. Phys. A 357 215.

[42] Wagner A. et al., 1998 Phys. Lett. B 420 20.

[43] Schwalb O. et al., 1994 Phys. Lett. B 321 20.

[44] Harris J. W. et al., 1985 Phys. Lett. B 153 377.

[45] T. Abbott et al. (E-802 Collaboration), Phys. Rev. C 50 (1993) 1024.

[46] J. Bachler et al., Phys. Rev. Lett. 72 (1994) 1419.

[47] Jacobs P. and NA49 Collaboration 1997 Proc. of the 3rd Int. Conf. on the Physics and Astrophysics of the Quark Gluon Plasma (Jaipur, India) (Delhi: Narosa).

[48] W. Reisdorf et al. (FOPI Collaboration), Nucl. Phys. A 781, 459 (2007).

[49] A.R. Wolf et al. (TAPS Collaboration), Phys. Rev. Lett. 80, 5281 (1998).

[50] R. Averbeck et al., Phys. Rev. C 67, 024903 (2003).

[51] J.L. Klay et al. (E895 Collaboration), Phys. Rev. C 68, 054905 (2003).

[52] R. Barth et al. Phys. Rev. Lett. 78 (1997), p. 4007.

[53] L. Ahle et al. (E802 Collaboration), Phys. Rev. C 60, 044904 (1999).

[54] L. Ahle et al. (E802 Collaboration), Phys. Rev. C 58, 3523 (1998).

[55] Afanasiev S. V. et al., Phys. Rev. C. 66 054902 (2002).

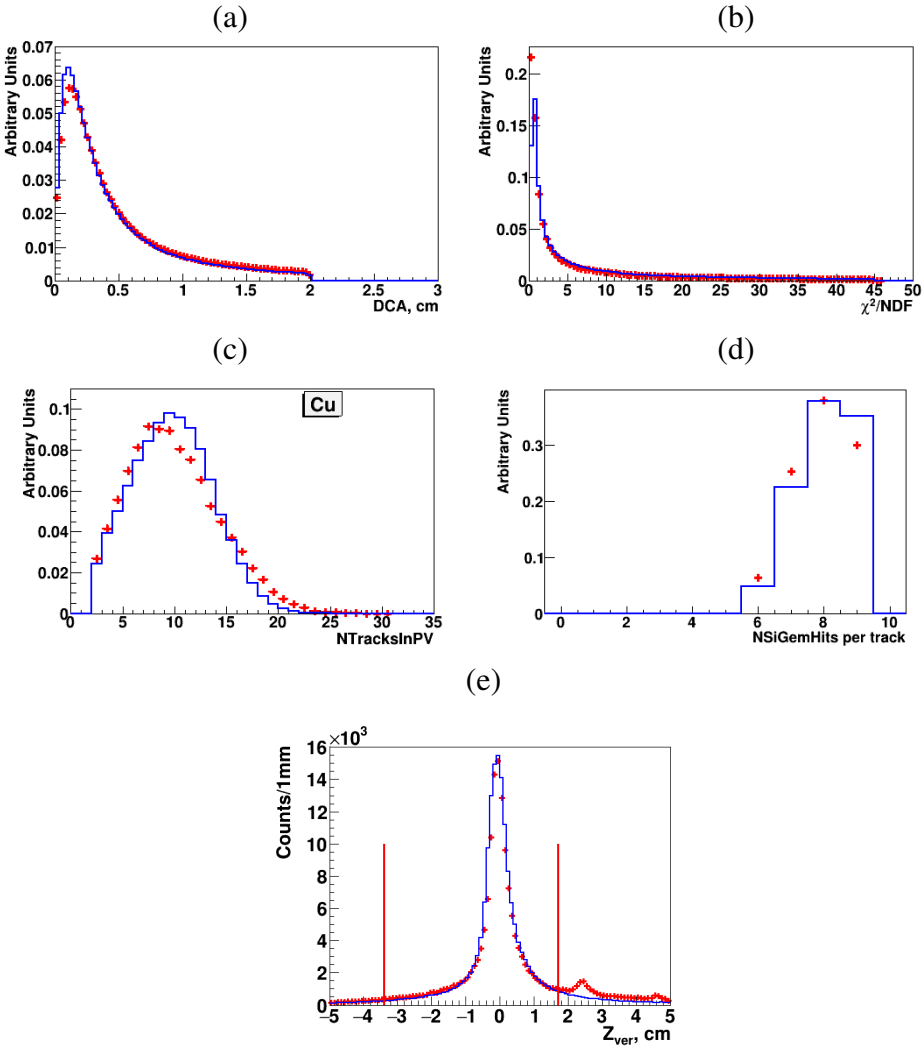


Figure 7: Ar+A interactions at 3.2 AGeV : comparison of the experimental distributions (red crosses) and reconstructed Monte Carlo GEANT distributions of events generated with the DCM-SMM model (blue lines): DCA; $\chi^2$/NDF of reconstructed tracks; number of tracks reconstructed in the primary vertex; number of hits per track reconstructed in 3 forward silicon and 6 GEM detectors; primary vertices along the Z axis for data and simulated events (vertical lines limit the Z region taken for the data analysis).

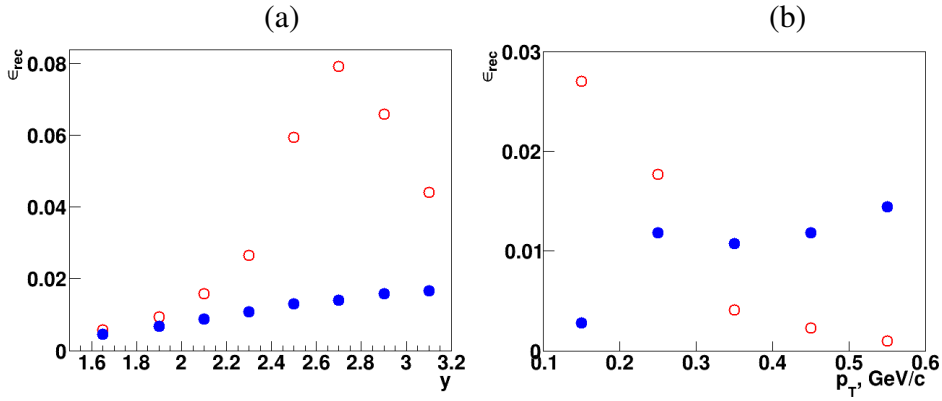


Figure 8: Reconstruction efficiency of $\pi^+$ detected in ToF-400 (open red circles) and ToF-700 (full blue circles), calculated as a product of the geometrical acceptance, detector efficiency and efficiency of kinematic and spatial cuts in bins of the rapidity $y$ in the laboratory frame (a) and in bins of $p_T$ (b). The results are shown for $\pi^+$ mesons produced in Ar+Sn interactions.

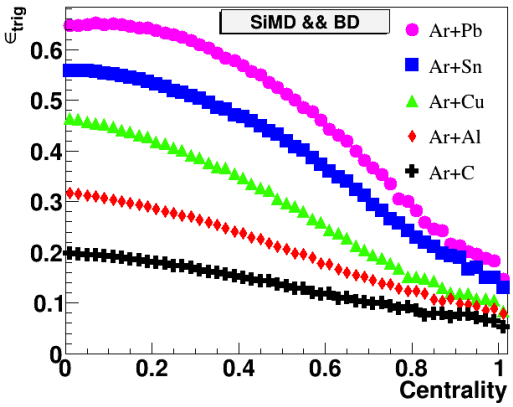


Figure 9: Trigger efficiency for interactions of the argon beam with various targets (C, Al, Cu, Sn, Pb) as a function of the event centrality estimated from the simulation.

Table 2: 1) Extrapolation coefficients for $\pi^+$ and $K^+$ meson multiplicities from the measured range to the entire kinematical range. The coefficients are averaged over predictions of the DCM-SMM, PHSD, UrQMD models. Uncertainties are taken as the maximal differences of the predictions of the models from the averaged values. 2) Number of participant nucleons from predictions of the DCM-SMM model. 3) Inclusive cross sections for inelastic Ar+A interactions.

| 3.2 AGeV argon beam | Ar+C | Ar+Al | Ar+Cu | Ar+Sn | Ar+Pb |
|---|---|---|---|---|---|
| Extrap. coeff. for $\pi^+$ | $3.25 \pm 0.18$ | $3.73 \pm 0.13$ | $4.45 \pm 0.07$ | $5.12 \pm 0.26$ | $5.91 \pm 0.55$ |
| Extrap. coeff. for $K^+$ | $2.81 \pm 0.66$ | $3.02 \pm 0.67$ | $3.34 \pm 0.65$ | $3.7 \pm 0.58$ | $4.1 \pm 0.43$ |
| $A_{\rm part}$, DCM-SMM | 14.8 | 23.0 | 33.6 | 48.3 | 63.6 |
| $\sigma_{inel}$, mb [29] | $1470 \pm 50$ | $1860 \pm 50$ | $2480 \pm 50$ | $3140 \pm 50$ | $3940 \pm 50$ |

Table 3: $\pi^+$ and $K^+$ meson multiplicities measured in Ar+C, Al, Cu, Sn, Pb interactions at the argon beam energy of 3.2 AGeV. The first error given is statistical, the second error is systematic. The third error given for the full $\pi^+$ and $K^+$ multiplicities is the model uncertainty.

| 3.2 AGeV argon beam | Ar+C | Ar+Al | Ar+Cu | Ar+Sn | Ar+Pb |
|---|---|---|---|---|---|
| Measured $\pi^+$ mult. $N_{\pi+}$ | $0.42 \pm 0.008 \pm 0.045$ | $1.00 \pm 0.01 \pm 0.07$ | $1.14 \pm 0.01 \pm 0.08$ | $1.28 \pm 0.01 \pm 0.09$ | $1.25 \pm 0.01 \pm 0.08$ |
| Measured $K^+$ mult. $N_{K+}/10^{-2}$ | $1.59 \pm 0.29 \pm 0.65$ | $3.90 \pm 0.28 \pm 0.61$ | $4.17 \pm 0.21 \pm 0.66$ | $5.60 \pm 0.22 \pm 0.75$ | $5.10 \pm 0.22 \pm 0.92$ |
| Full $\pi^+$ mult. $N^{tot}_{\pi+}$ | $1.365 \pm 0.026 \pm 0.146 \pm 0.08$ | $3.73 \pm 0.04 \pm 0.26 \pm 0.13$ | $5.07 \pm 0.04 \pm 0.36 \pm 0.08$ | $6.55 \pm 0.05 \pm 0.46 \pm 0.33$ | $7.39 \pm 0.06 \pm 0.47 \pm 0.69$ |
| Full $K^+$ mult. $N^{tot}_{K+}/10^{-2}$ | $4.47 \pm 0.81 \pm 1.83 \pm 1.05$ | $11.8 \pm 0.9 \pm 1.8 \pm 2.6$ | $13.9 \pm 0.7 \pm 2.2 \pm 2.7$ | $20.7 \pm 0.8 \pm 2.8 \pm 3.3$ | $20.9 \pm 0.9 \pm 3.8 \pm 2.2$ |
| $N_{K+}/N_{\pi+}/10^{-2}$ Measured range | $3.79 \pm 0.69 \pm 1.52$ | $3.90 \pm 0.28 \pm 0.55$ | $3.66 \pm 0.19 \pm 0.53$ | $4.39 \pm 0.18 \pm 0.51$ | $4.11 \pm 0.18 \pm 0.68$ |
| $N^{tot}_{K+}/N^{tot}_{\pi+}$ $/10^{-2}$, Full kin. range | $3.27 \pm 0.6 \pm 1.38 \pm 0.79$ | $3.16 \pm 0.23 \pm 0.54 \pm 0.71$ | $2.75 \pm 0.14 \pm 0.48 \pm 0.54$ | $3.16 \pm 0.13 \pm 0.48 \pm 0.52$ | $2.83 \pm 0.12 \pm 0.54 \pm 0.39$ |
| $K^+$ inv. slope $T_0$, MeV, Meas. range | $67 \pm 12 \pm 12$ | $80 \pm 7 \pm 5$ | $81 \pm 5 \pm 5$ | $81 \pm 5 \pm 4$ | $78 \pm 5 \pm 4$ |

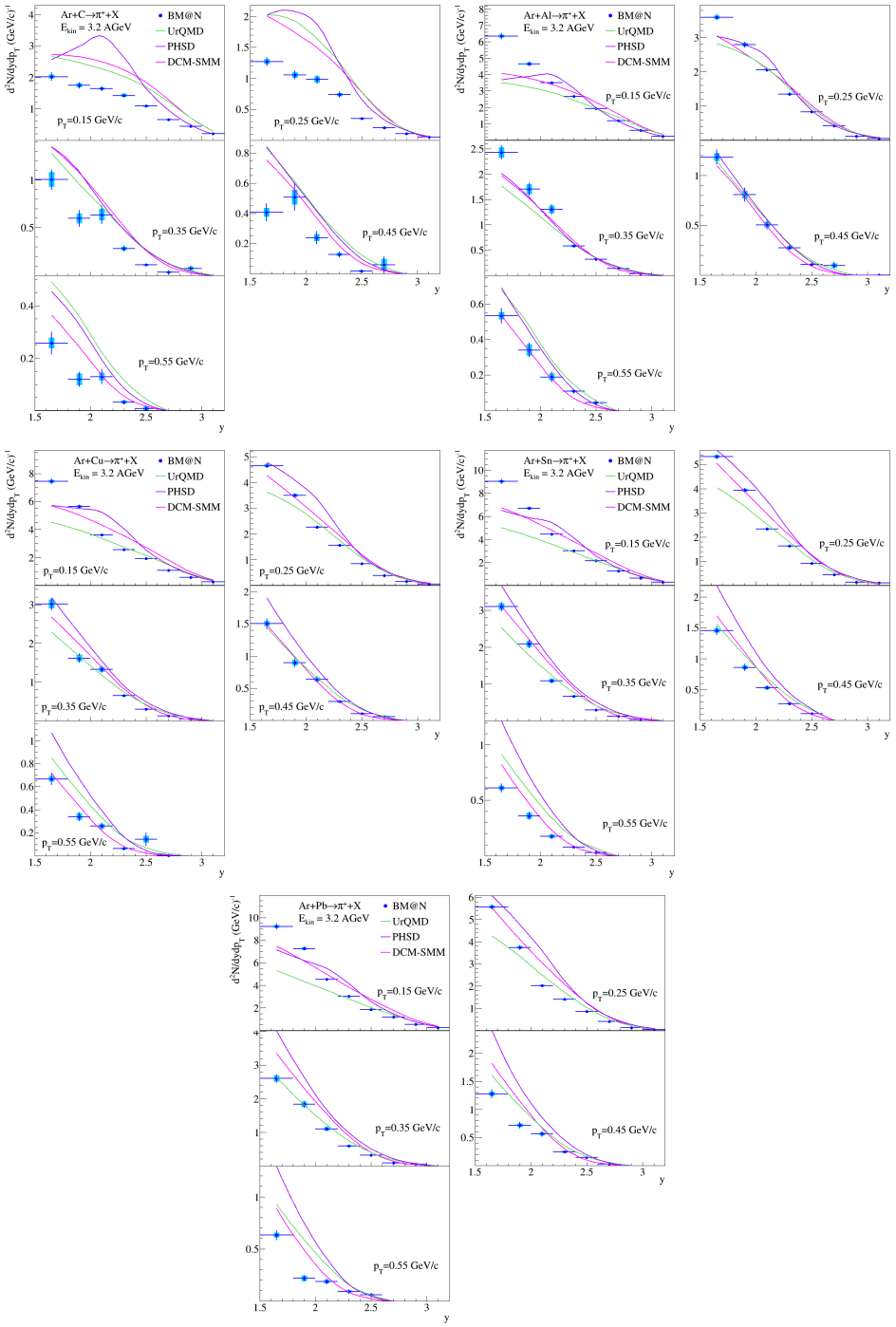


Figure 10: Rapidity spectra ($y$) of $\pi^+$ mesons produced in Ar+C, Al, Cu, Sn, Pb interactions at the argon beam energy of 3.2 AGeV. The results are given for bins of $\pi^+$ meson transverse momentum. The error bars represent the statistical errors, the boxes show the systematic errors. The predictions of the DCM-SMM, UrQMD and PHSD models are shown as rose, green and magenta lines.

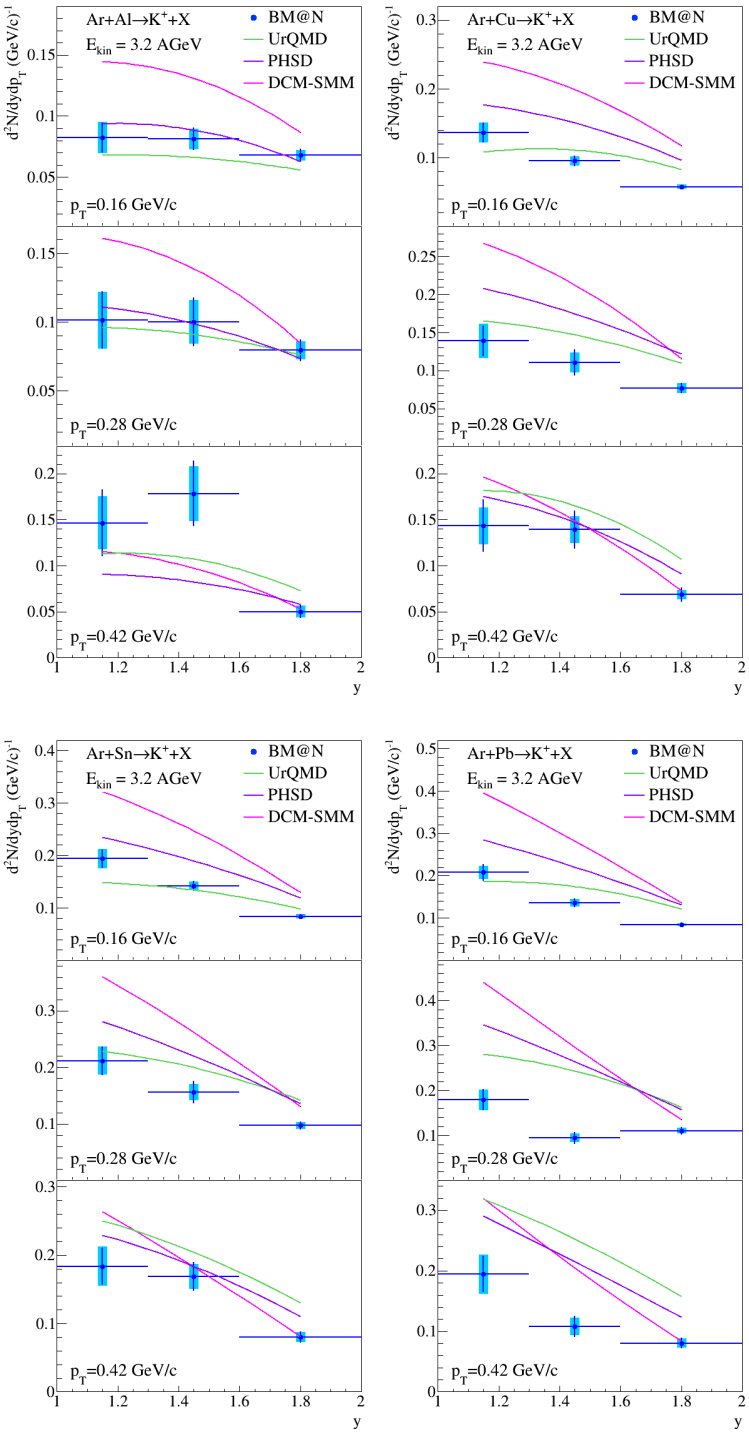


Figure 11: Rapidity spectra ($y$) of $K^+$ mesons produced in Ar+Al, Cu, Sn, Pb interactions at the argon beam energy of 3.2 AGeV. The results are given for bins of $K^+$ meson transverse momentum. The error bars represent the statistical errors, the boxes show the systematic errors. The predictions of the DCM-SMM, UrQMD and PHSD models are shown as rose, green and magenta lines.

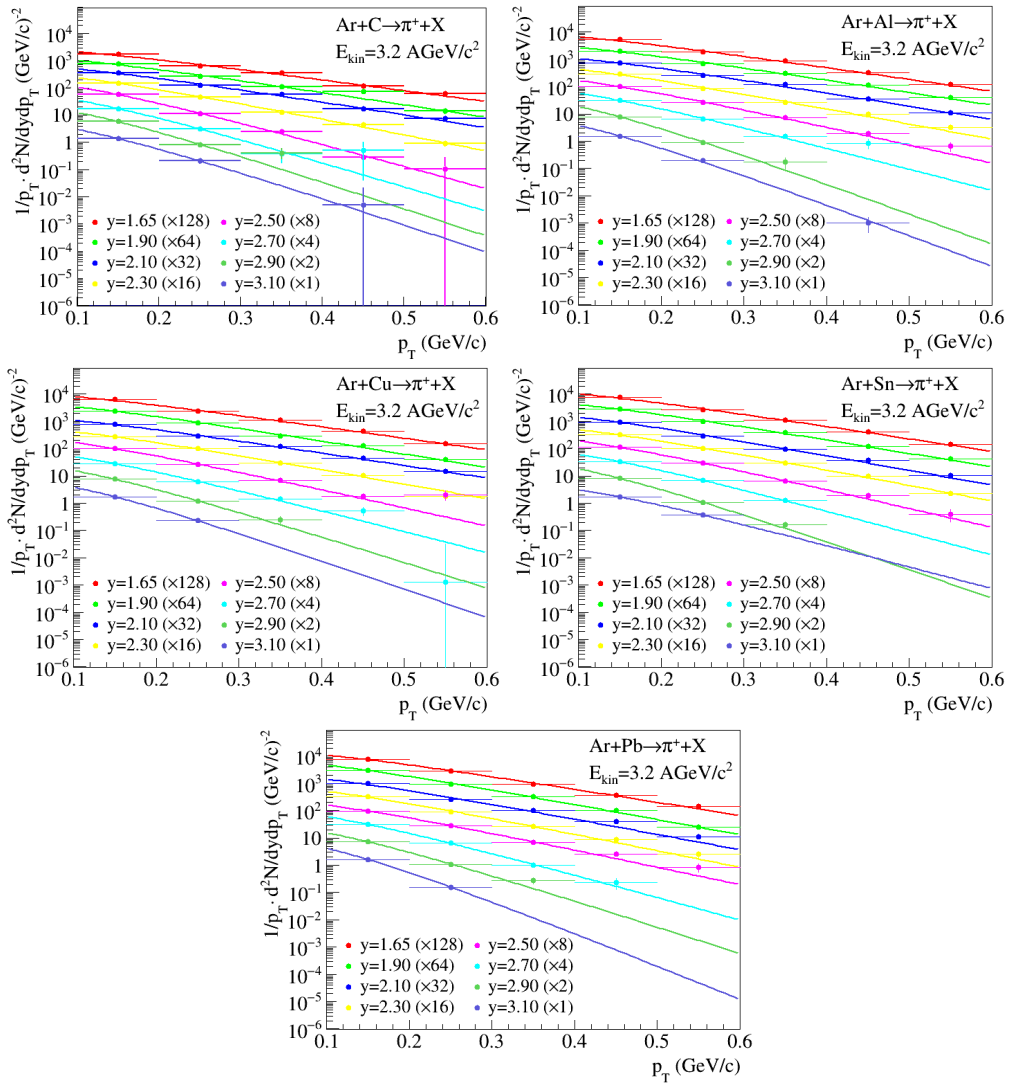


Figure 12: Transverse momentum spectra ($p_T$) of $\pi^+$ mesons produced in Ar+C, Al, Cu, Sn, Pb interactions at the argon beam energy of 3.2 AGeV. The results are given for bins of $\pi^+$ meson rapidity. The lines represent the results of the parameterization described in the text.

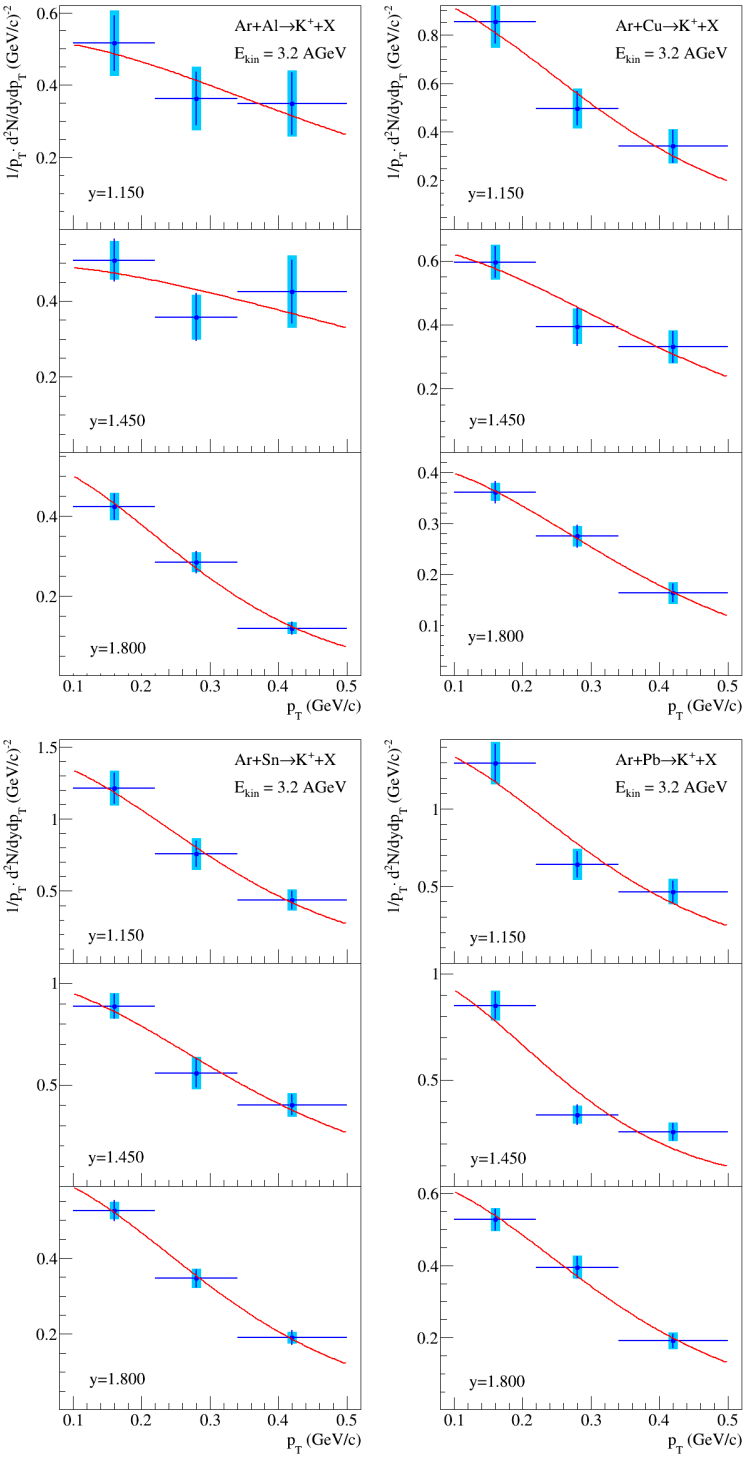


Figure 13: Transverse momentum spectra ($p_T$) of $K^+$ mesons produced in Ar+Al, Cu, Sn, Pb interactions at the argon beam energy of 3.2 AGeV. The results are given for three bins of $K^+$ meson rapidity. The error bars represent the statistical errors, the boxes show the systematic errors. The lines represent the results of the parameterization described in the text.

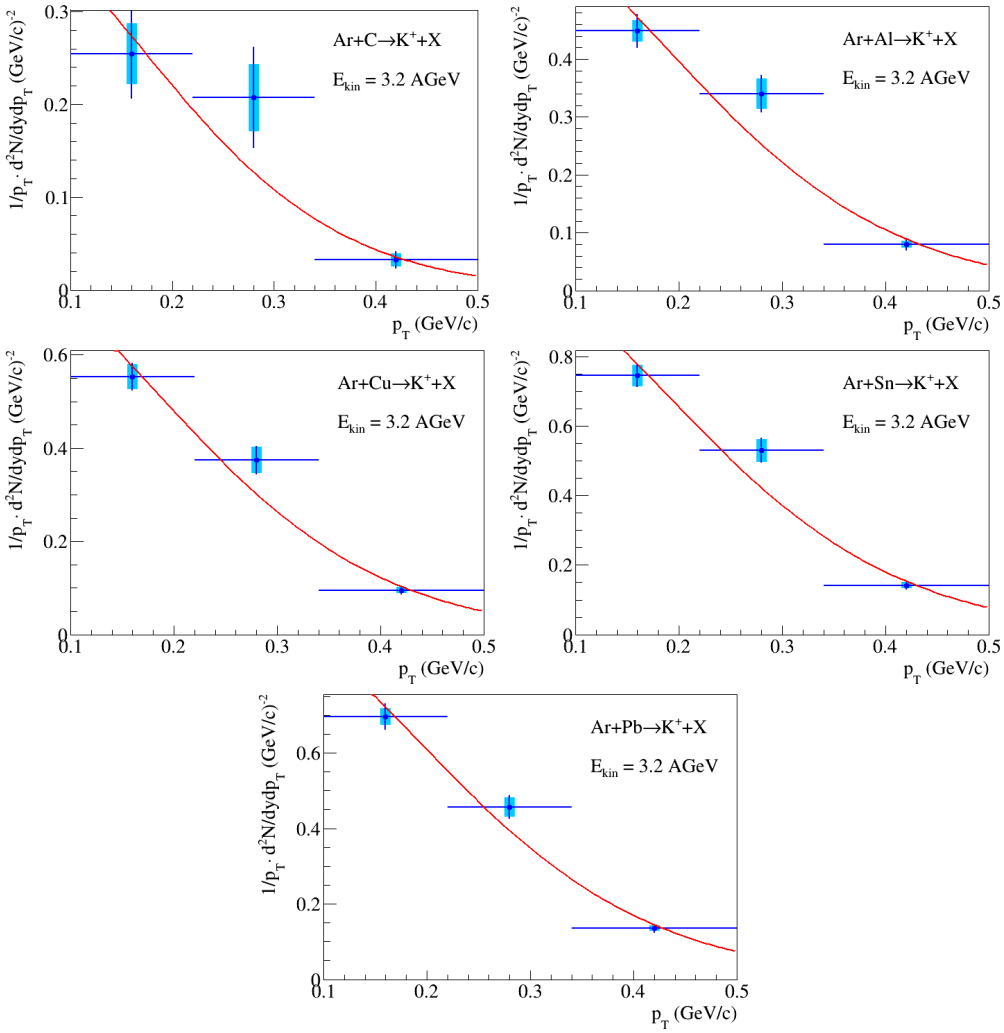


Figure 14: Transverse momentum spectra ($p_T$) of $K^+$ mesons produced in Ar+C, Al, Cu, Sn, Pb interactions at the argon beam energy of 3.2 AGeV. The results are given for the measured $K^+$ meson rapidity range. The error bars represent the statistical errors, the boxes show the systematic errors. The lines represent the results of the parameterization described in the text.

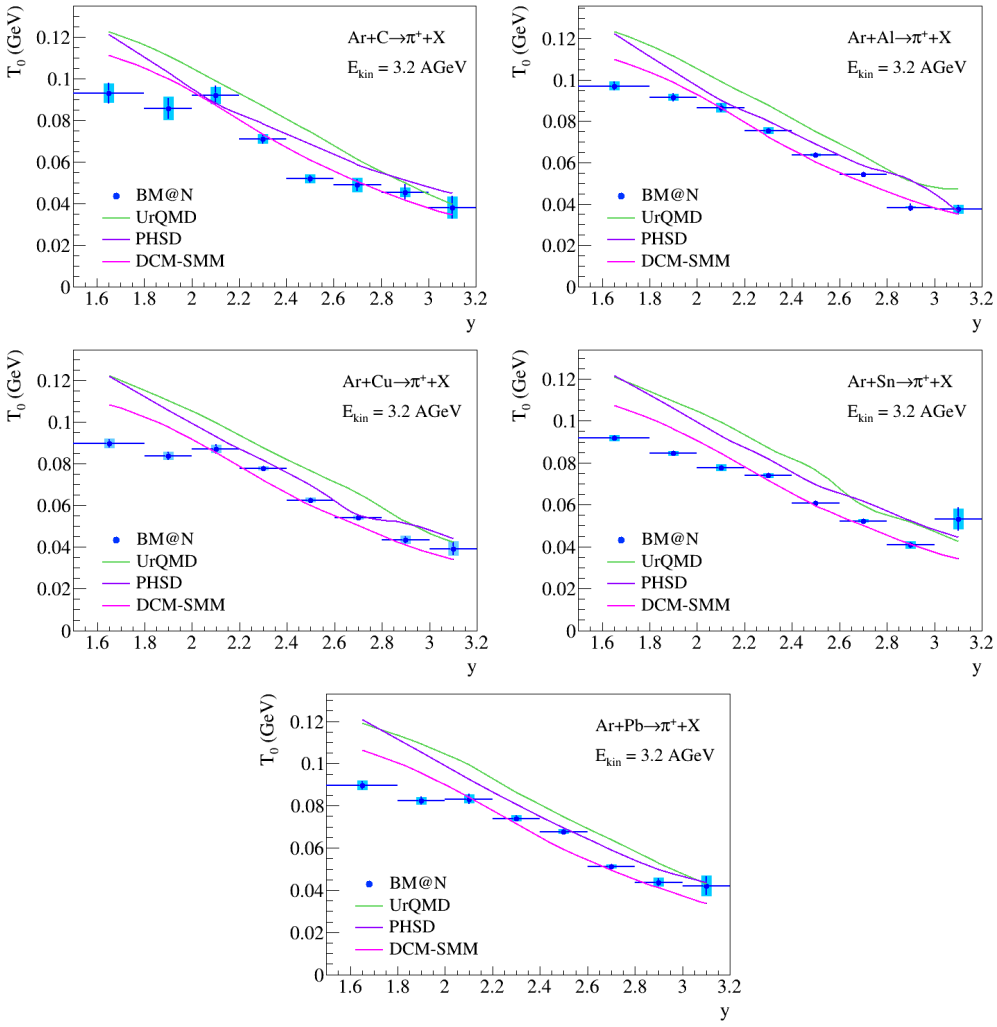


Figure 15: Rapidity $y$ dependence of the inverse slope $T_0$ determined from the fits of the $\pi^+$ $p_T$ spectra in Ar+C, Al, Cu, Sn, Pb interactions. The error bars represent the statistical errors, the boxes show the systematic errors. The predictions of the DCM-SMM, UrQMD and PHSD models are shown as rose, green and magenta lines.

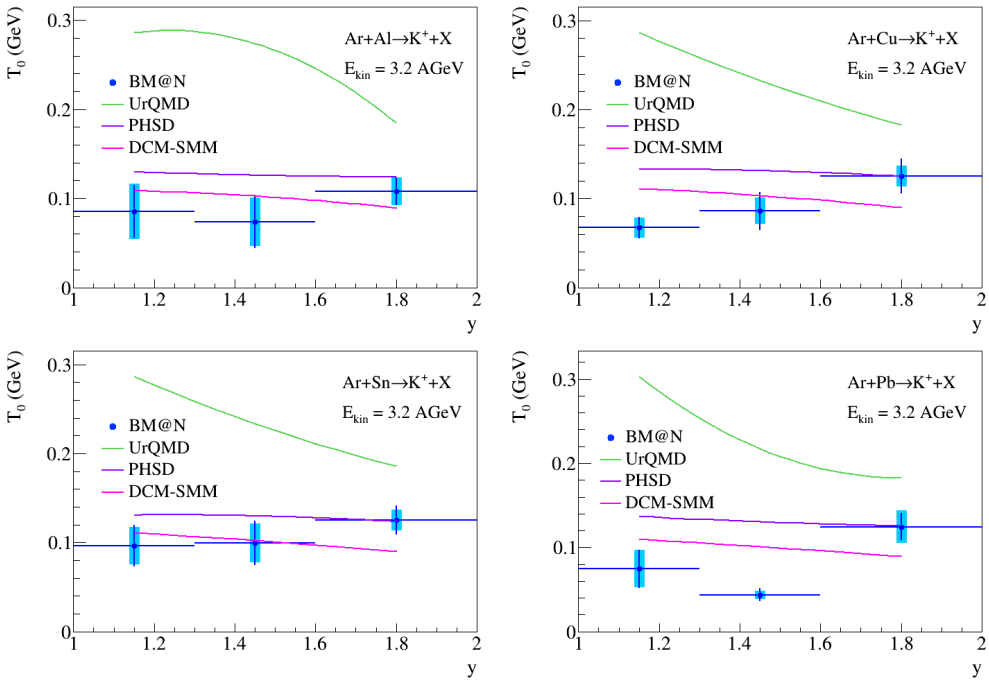


Figure 16: Rapidity $y$ dependence of the inverse slope $T_0$ extracted from the fits of the $K^+$ $p_T$ spectra in Ar+Al, Cu, Sn, Pb interactions. The error bars represent the statistical errors, the boxes show the systematic errors. The predictions of the DCM-SMM, UrQMD and PHSD models are shown as rose, green and magenta lines.

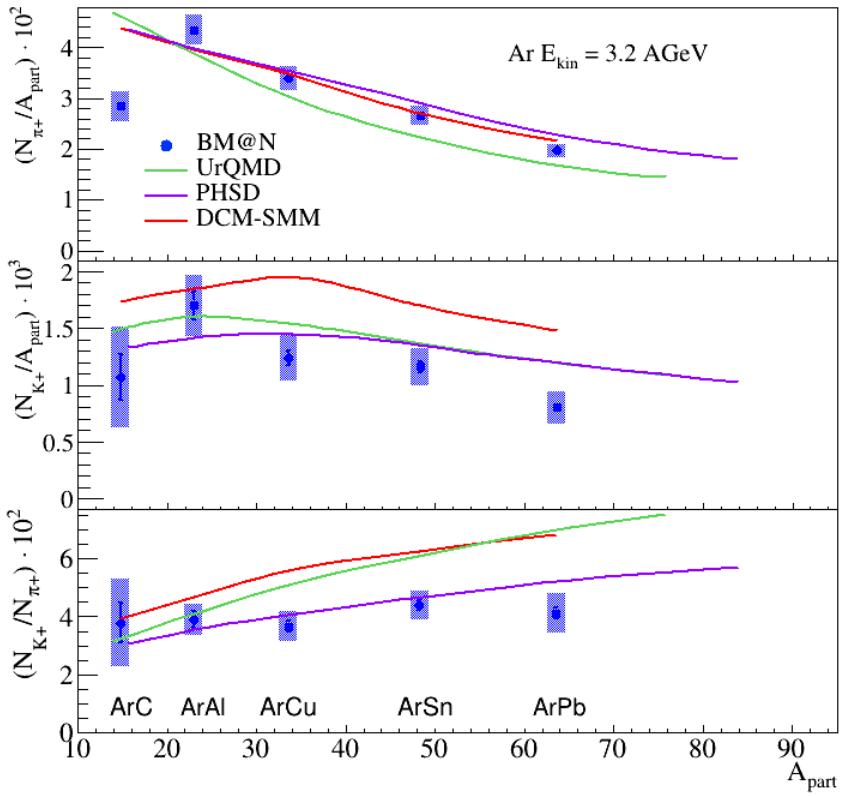


Figure 17: Ratios of the $\pi^+$ (a) and $K^+$ (b) multiplicities to the number of participant nucleons and ratios of the $K^+$ to $\pi^+$ multiplicities (c) in the measured kinematical range in Ar+C, Al, Cu, Sn, Pb interactions. The error bars represent the statistical errors, the blue boxes show the systematic errors. The BM@N results are compared with predictions of the DCM-QGSM, UrQMD and PHSD models for argon-nucleus interactions shown as red, green and magenta lines.

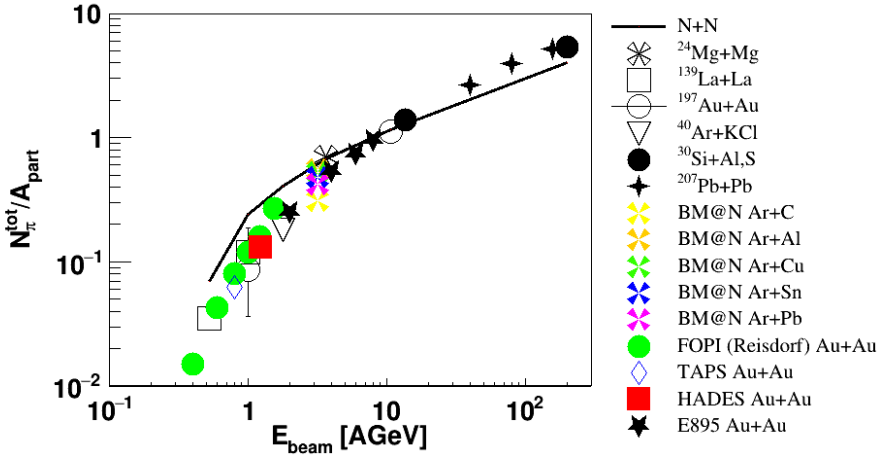


Figure 18: Pion multiplicity $N_\pi^{tot}$ per the mean number of participant nucleons $A_{\rm part}$ shown as a function of the beam kinetic energy $E_{\rm beam}$. The BM@N results are compared with the world measurements (references in the text).

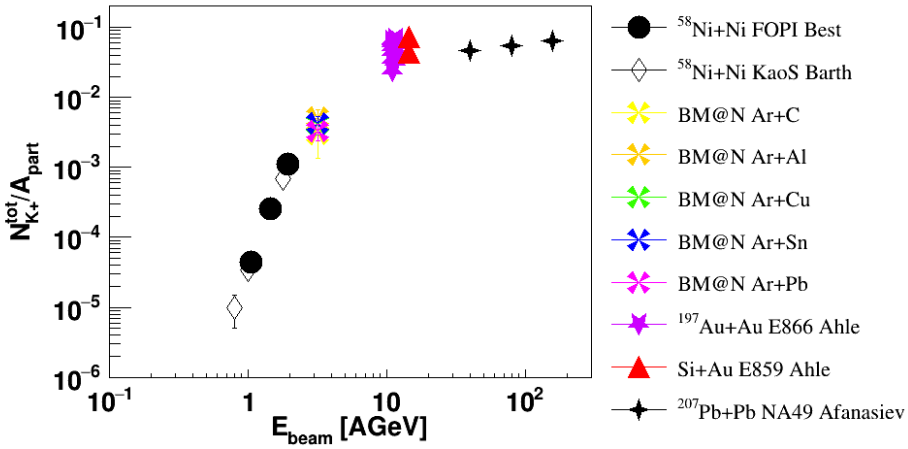


Figure 19: $K^+$ multiplicity per the mean number of participant nucleons $A_{\rm part}$ shown as a function of the beam kinetic energy $E_{\rm beam}$. The BM@N results are compared with the world measurements (references in the text).